INTERNATIONAL JOURNAL OF HYDROGEN ENERGY 45 (2020) 10951–10961

Available online at www.sciencedirect.com

ScienceDirect

journal homepage: www.elsevier.com/locate/he

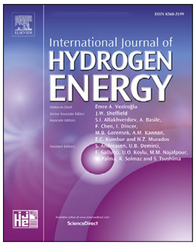

Effects of alloy compositions on hydrogen behaviors at a nickel grain boundary and a coherent twin boundary

Jun Hui [a,1], *Guo Yang* [b,1], *Min Liu* [a], *Wenguan Liu* [a,b,*], *Biao Wang* [a,**]

[a] *Sino-French Institute of Nuclear Engineering and Technology, Sun Yat-Sen University, Zhuhai, 519082, China*
[b] *Shanghai Institute of Applied Physics, Chinese Academy of Sciences, Shanghai, 201800, China*

HIGHLIGHTS

- Effects of common elements on H were studied by first-principles calculations.
- Both Ni grain boundary (GB) and coherent twin boundary (CTB) were studied.
- Effects of alloying elements on energetics and kinetics of H were studied.
- The effects were decomposed into physical and chemical components.
- The mechanisms at electronic and atomic levels were explored.

ARTICLE INFO

Article history:
Received 23 September 2019
Received in revised form
31 January 2020
Accepted 3 February 2020
Available online 22 February 2020

Keywords:
First-principles calculation
Hydrogen
Nickel
Alloy composition
Grain boundary
Coherent twin boundary

ABSTRACT

The effects of several common metallic and nonmetal alloy compositions (i.e., Cr, Mo, B, and P) on the energetics and kinetics of hydrogen behaviors at a nickel grain boundary (GB) and a coherent twin boundary (CTB) were systematically investigated by first-principles calculations. H, Cr, Mo, B, and P have a stronger segregation into Ni GB than Ni CTB due to the presence of a cavity in GB. Cr, Mo, B, and P all act as obstacles for H segregation and diffusion in both GB and CTB, but the physical mechanisms are different: In Ni GB, Cr and Mo result in the shrinkage of isosurfaces of optimal charge densities for H, and B and P provide a strong competitive tendency to accumulate into the GB; in Ni CTB, Cr and Mo induce charge accumulation, and B and P result in a repulsive interaction to H. The present study provides the microscopic images of H compositions in Ni GB and CTB under the effects of alloy compositions; this is essential for understanding the mechanism of hydrogen embrittlement (HE) and improving the ability of alloys against HE.

---

* *Corresponding author*. Sino-French Institute of Nuclear Engineering and Technology, Sun Yat-Sen University, Zhuhai, 519082, China.
** *Corresponding author*.
E-mail addresses: liuwg7@mail.sysu.edu.cn (W. Liu), wangbiao@mail.sysu.edu.cn (B. Wang).

[1] co-first author.

https://doi.org/10.1016/j.ijhydene.2020.02.008

Introduction

Hydrogen embrittlement (HE) [1–3] in metals and alloys has been extensively researched for many decades, and is normally not detectable before the final fracture of metals and alloys. HE is a complex phenomenon, and there are a variety of mechanisms that are responsible for HE of a material [4–7]. HE involves the interactions between hydrogen and defects at multiple-length scales [8–11], and our understanding of HE is limited by the challenge of measuring the precise location of H atoms [8,9]. Recently, Chen et al. [8,12] used cryo-transfer atom probe tomography to observe H at specific microstructural features in steels and directly observed hydrogen at dislocations and grain boundaries that can act as trapping sites.

Nickel-based alloys are important commercial alloy that have widespread applications according to their excellent mechanical properties, high-temperature performance, and corrosion resistance. Nevertheless, Ni-based alloys are susceptible to HE [3,13–15], which impairs their excellent performance. In addition to the experimental studies, first-principles calculations are very suitable to study H behaviors in alloys fundamentally and have already been extensively utilized to investigate the HE of the Ni metal and Ni alloys, e.g., H on the Ni surface [16,17], H diffusion in Ni [18–20], and H in the vacancy of Ni [21–25], in which first-principles calculations can not only provide a deep understanding of the HE mechanism but also predict the susceptibility of metals and alloys toward HE.

As is well known, H trapping and diffusion at the Ni grain boundary (GB) are crucial for HE phenomena, and GB serves as an area for accumulation of H atoms and diffusion of a rapid channel. Thus, first-principles calculations have been extensively used to study H behaviors in NiΣ5 GB [13–15,26–30], which is a representative kind of Ni GB, since both substitutional and interstitial sites exist on the Σ5 GB plane for the alloying elements because of the presence of a cavity in the GB region. Zhu et al. [13] mainly studied the effects of several metallic elements (i.e., Al, Ta, W, and Zr) on H in Ni GB using first-principles calculations and found that the elements can act as an obstacle for H diffusion at Ni GBs.

In particular, among various kinds of GBs, the Ni coherent twin boundary (CTB) is quite special, and it is also called Σ3 GB in some cases. CTB is simply a special GB. For simplicity, "GB" only indicates Σ5 GB in the following sections. CTB is in an FCC structure, as the (111) mirror planes where the normal stacking sequence of (111) planes is reversed and has the amazing ability to improve the strength and ductility of alloys simultaneously [31–34]. Recently, Zhou et al. [35] used first-principles calculations to reveal that the studied metallic elements (i.e., Al, Cr, Mo, Nb, and Ti) can considerably increase the formation of vacancies and vacancy-hydrogen clusters at Ni CTB, which may facilitate nanovoid nucleation to promote final crack initiation at Ni CTBs.

In Ni alloys, alloy compositions can modify H behavior, thus serving as an engineering approach to solving the HE problem. As a result, the effects of alloy compositions on H behavior are essential for understanding the HE mechanism and improving the ability of alloys against HE in commercial Ni alloys. Unfortunately, the present studies mainly focus on H behavior in pure Ni bulk or GB without considering the effects of alloy compositions except a few studies as mentioned above [13,28,35].

In our previous studies, we have investigated the interactions between H and 3d/4d transition elements, sp-elements in the bulk of Ni alloys through first-principles calculations [36–38], and in this study, we further studied the effects of several representative alloy compositions (not only metallic elements but also nonmetal elements) on H trapping and diffusion at Ni GBs and CTBs. The chosen alloy compositions in this work consisted of Cr, Mo, B, and P. Cr and Mo represent transition elements that are common and are major elements in Ni alloys. B and P are the universal nonmetal elements that exist in almost all alloys, not just in Ni alloys.

Computational methods

The Vienna ab-initio simulation package (VASP) [39] was employed to perform spin-polarized electronic state calculations within the density functional theory [40,41]. Electron-ion interactions were described by the projector-augmented plane-wave (PAW) [42] method and the wave functions were expanded in a plane-wave basis set with a cutoff energy of 450 eV. A generalized gradient approximation (GGA) [43] of the exchange correlation energy was used in PBE scheme. Total energy and Hellmann–Feynman forces were convergent within 10^{-6} eV and 10^{-2} eV/Å, respectively. The Monkhorst-Pack k-point meshes of $4 \times 8 \times 2$ for NiΣ5 GB and $6 \times 10 \times 1$ for Ni CTB model were used to sample the Brillouin zone [44]. Ni GB and CTB are model based on the optimized lattice parameter, 3.522 Å, of the FCC Ni, which is in good agreement with the experimental value when extrapolated from room temperature to 0 K (3.517 Å) [18,37].

To evaluate the energy barrier of H diffusion in pure and alloyed GB and CTB, the climbing image nudged elastic band method (cNEB [45,46]) was utilized to calculate the potential barrier and transition state (TS) for H diffusion across or along GB and CTB, with the force tolerance of 10^{-2} eV/Å. In each process of H diffusion, a total of three images are used (not including the initial and final images).

The GB model contains a cavity, which is different from CTB, as illustrated in Fig. 1. In the GB plane, "0" refers to the cavity in GB, i.e., the GB0 site. Twenty atomic layers are included, and each layer consists of two equivalent atomic sites. The calculated dimensions of the GB model are $7.80 \times 3.48 \times 16.63$ Å^3. The CTB in a face-centered cubic structure is an anti-stacked sequence to the substrate material along the [111] direction [31]. In the Ni CTB model illustrated in Fig. 1(a), 12 atomic layers are contained, and each layer consists of two equivalent atomic sites. The calculated size of the CTB model is $4.31 \times 2.49 \times 24.46$ Å^3. The same numeric planes in both sides of GB and CTB are symmetric.

To identify a site that is favored energetically for the alloying atoms to occupy, the binding energy of one alloying atom in GB or CTB, E_A^b, is defin0065d as follows [30,47]:

$$E_A^b = E_{NT/GB}(N_{Ni}, 1) - E_A - E_{NT/GB}\left(N_{Ni}^0\right) - \frac{N_{Ni} - N_{Ni}^0}{N_{Ni}^0} E_{Bulk}\left(N_{Ni}^0\right), \tag{1}$$

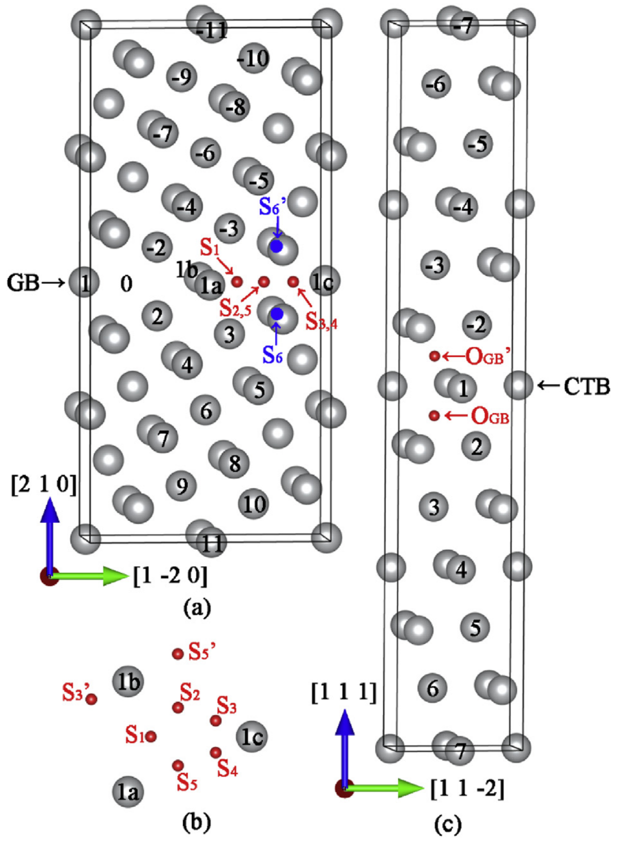

Fig. 1 – (a) The NiΣ5 GB model, (b) the possible interstitial sites of H in the GB plane of (a) and (c) the Ni CTB model. "GB" in (a) indicates the GB plane, and "CTB" in (b) denotes the CTB plane. The atomic layers are labeled by numbers counted from the GB or CTB plane in (a) and (b), and "0" in (a) denotes the cavity in Σ5 GB. In (b), S2 and S5 sites are at equivalent positions, and S3 and S4 sites are also at equivalent positions. S1, S2/S5, and S3/S4 sites are in one cavity of the GB plane surrounded by 1a, 1b, and 1c atoms, and S3′ and S5′ sites are out of this cavity and within the adjacent ones.

where $E_{NT/GB}(N_{Ni}, 1)$ refers to the calculated total energy of the GB or CTB unit cell including N_{Ni} Ni atoms and one alloying atom, E_A is the energy of one isolated alloying atom, and N^0_{Ni} is the number of Ni atoms in the clean GB or CTB and bulk unit cells. For $N_{Ni} = N^0_{Ni} - 1$, the last term is used to adjust the number of Ni atoms when one alloying atom is substituted for the Ni atom. The tendency for the alloying atom to diffuse from a bulk site to a GB or CTB site can be quantified by the segregation energy, ΔE^{Seg}_A, which was calculated as

$$\Delta E^{Seg}_A = E^b_A - E^b_{Bulk-A}, \tag{2}$$

where E^b_{Bulk-A} is the binding energy of one alloying atom in the bulk site of GB or CTB.

The binding energy for one H atom, E^b_H, was defined as

$$E^b_H = E_{GB/CTB+H} - E_{GB/CTB} - \frac{1}{2}E_{H2}, \tag{3}$$

where $E_{GB/CTB+H}$ or $E_{GB/CTB}$ is the total energy of the GB/CTB supercell with or without an H atom, and E_{H2} is the energy of an isolated H_2 molecule. The segregation energy of the H atom, ΔE^{Seg}_H, is calculated as

$$\Delta E^{Seg}_H = E^b_H - E^b_{Bulk-H}, \tag{4}$$

where E^b_{Bulk-H} is the binding energy of one H atom in the bulk site of pure GB or CTB (i.e., the octahedral interstitial site), which is the most stable site for H in Ni bulk [37].

The binding energy and segregation energy of alloy compositions (i.e., Cr, Mo, B, and P) were calculated to identify the occupation position of alloy compositions in GB and CTB, and the negative values imply a preferable occupation and segregation of H atoms. Then, H behaviors of trapping and diffusion in Ni GB and Ni CTB with or without segregated alloy compositions were investigated to explore the role of alloy composition on H atoms. For simplicity, Cr-segregated Ni GB and CTB are denoted as Ni/Cr GB and Ni/Cr CTB, respectively; this is also applicable to the cases of the other elements.

Results and discussion

Segregation of alloy compositions at the GB and CTB

To find out which site is preferable for alloy composition, the binding energies and segregation energies for Cr, Mo, B, and P at each atomic site in the Ni GB and CTB models were calculated and demonstrated in Figs. 2 and 3, respectively. A negative value of the binding energy or segregation energy indicates a segregation tendency at the GB or CTB.

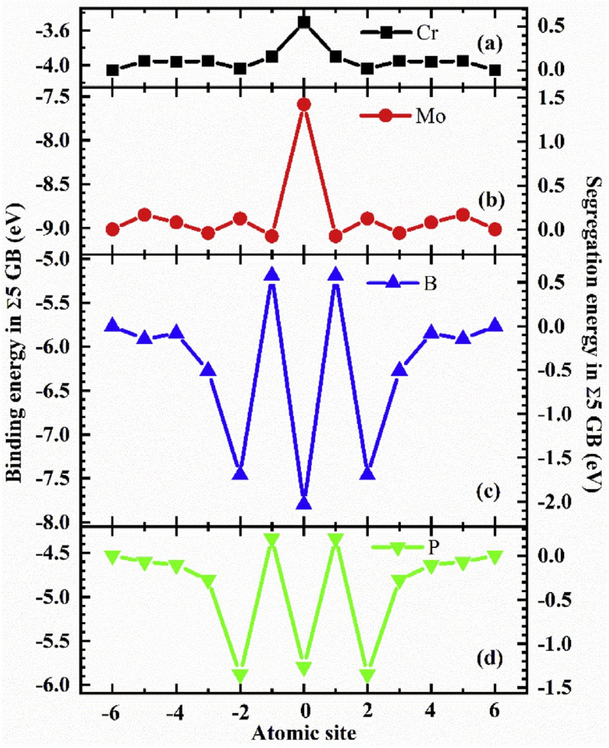

Fig. 2 – Calculated binding energies and segregation energies for (a) Cr, (b) Mo, (c) B, and (d) P at each atomic site in the Ni GB model illustrated in Fig. 1(a).

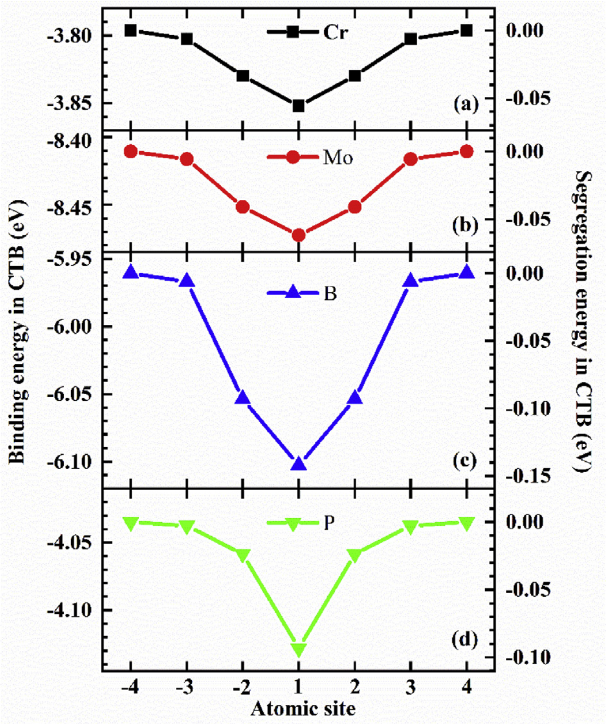

Fig. 3 – Calculated binding energies and segregation energies for (a) Cr, (b) Mo, (c) B, and (d) P at each atomic site in the Ni CTB model illustrated in Fig. 1(c).

The Ni GB model contains both the cavity site (i.e., GB0 in Fig. 1(a)) and substitutional sites (e.g., ±GB1 and ±GB2 in Fig. 1(a)). It can be judged from Fig. 2 that GB0 is unfavorable for Cr and Mo with the largest binding energy (0.55 and 1.42 eV, respectively), which is directly associated with the small size of the GB0 site. For the case of Cr in Fig. 2(a), there are no obvious differences of segregation tendency in the substitutional sites. For the case of Mo in Fig. 2(b), the GB1 site is a slightly more preferred position.

By contrast, the nonmetal elements (B and P) have a strong tendency to segregate to the GB region. The GB0 site is most favorable for B energetically with segregation energy −2.03 eV in Fig. 2(c). GB0 and GB2 sites are most preferred for P with the segregation energy −1.26 and −1.35 eV, respectively, which is in good agreement with our previous work [48]. When all of the sites in the GB0 or GB1 layer are occupied by P atoms in the Ni GB model, the segregation energy of the former is lower [48].

The Ni CTB model is coherent and without cavities as illustrated in Fig. 1(c); thus, only substitutional sites were investigated. As shown in Fig. 3, it is obvious that the atomic site 1 (i.e., CTB1 site in Fig. 1(c)) is most favorable for Cr, Mo, B, and P to occupy in the Ni CTB model. However, the corresponding segregation energies are small, with the values of −0.056, −0.062, −0.142 and −0.093 eV per atom, respectively, indicating that they have a relatively small segregation tendency to the CTB plane.

Throughout the following sections of this study, to investigate the effects of alloy compositions on hydrogen trapping and diffusion at Ni GB and CTB, H atoms are added on the basis of the segregation configurations with Cr or Mo atoms substituted in the GB1 sites of the Ni GB model, B or P atoms inserted in GB0 sites of the Ni GB model, and Cr, Mo, B or P atoms substituted in CTB1 sites of the Ni CTB model.

H trapping and diffusion in Ni GBs with alloy compositions

H at the Ni/Cr and Ni/Mo GBs

To study the effects of alloy compositions on H accumulation in the GB region, the binding energies of H atoms in various interstitial sites in and near the GB plane of the pure, Ni/Cr, and Ni/Mo GBs were calculated, as presented in Table 1. Our calculated segregation energies of H in pure Ni GB are in reasonable agreement with the results of Stefano [44]. As demonstrated in Fig. 1(a) and (b), sites S1–S5 are in the GB plane, and site S6 is the nearest H site to the GB plane. In Table 1, all of the H binding energies are negative, which means H atoms have the tendency to diffuse into the GB region and can be trapped in it. However, the values of the H binding energies are in the order pure GB > Ni/Cr > Ni/Mo, indicating that both Mo and Cr suppress H accumulation and segregation and that the effect of Mo is most apparent. Moreover, sites S3 and S4 are no longer stable for H atoms in Ni/Cr and Ni/Mo GBs, and the H atoms in the S3 and S4 sites will jump into the S2 and S5 sites; thus, there are only three stable atomic sites (i.e., S1, S2, and S5) in one cavity of the GB plane surrounded by the atoms in the sites 1a, 1b, and 1c illustrated in Fig. 1(b).

As listed in Table 1, the S2 and S5 sites are the most stable in Ni/Cr and Ni/Mo GBs, and Cr and Mo change the binding energies and segregation energies by −0.01 and 0.12 eV, respectively, compared with those in pure GB. Hence, to deeply understand the suppression effect of Mo and Cr on H segregation, the changes of binding energies and segregation energies in the S2 and S5 sites can be decomposed into chemical and mechanical components [47,49,50]. The calculated results are illustrated in Table 2, in which a positive value means the suppression of H segregation, and a negative one denotes a promotion effect.

Table 1 – The calculated binding energies and segregation energies (in eV) of one H atom at the pure, Ni/Cr, and Ni/Mo GBs. The segregation energies are in parentheses. (See Fig. 1(a) and (b) to find the positions of interstitial sites of H, i.e., S1, S2, S3, S4, S5, and S6).

	Pure GB	Ni/Cr GB	Ni/Mo GB
S1	−0.18 (−0.24)	−0.13 (−0.18)	−0.03 (−0.09)
S2/S5	−0.17 (−0.22)	−0.18 (−0.23)	−0.05 (−0.10)
S3/S4	−0.05 (−0.10)	–	–
S6	−0.11 (−0.17)	−0.09 (−0.14)	0.02 (−0.04)

Table 2 – The calculated total effects of Cr and Mo on the H binding energies and segregation energies (in eV) in the S2 and S5 sites of Ni/Cr and Ni/Mo GBs and the corresponding chemical and mechanical components.

	Chemical	Mechanical	Total
At Ni/Cr GB	0.082	−0.095	−0.01
At Ni/Mo GB	0.39	−0.27	0.12

In Table 2, the chemical components for Cr and Mo are both positive and suppress H segregation. The chemical components are thought to be induced by the electronic distribution. The cavity in the GB plane provides an isosurface of optimal charge density for H atoms to bind on its internal surface [44,51], which has a close association with the chemical components, and the calculated isosurfaces of optimal charge densities for H in pure, Ni/Cr, and Ni/Mo GBs are displayed in Fig. 4. In Fig. 4(a), the isosurface is largest, and the stable sites for H atoms shown in Fig. 1(a) and (b), sites S1–S5, all bind onto an isosurface of the same charge density (0.14 electrons/Å^3). However, the isosurfaces shrink obviously in Fig. 4(b) and (c); this shrinkage is directly associated with the segregated Cr and Mo atoms, and sites S3 and S4 are no longer on the isosurface and become unstable for H atoms; this is in good agreement with the calculated binding energies in Table 1. The effect of Mo on the shrinkage of the isosurface is most distinct and thus suppresses H segregation, confirming the results of the chemical components in Table 2.

As shown in Table 2, the mechanical values of Cr and Mo are positive and promote H segregation. The mechanical components are closely associated with atomic size. The atomic size of Mo is obviously larger than that of Ni. Thus, Mo can induce the more obvious volume expansions in the GB region; this is beneficial for H segregation. However, the chemical component contributes the major part of the effect of Mo, and the mechanical one only reduces its value as displayed in Table 2. Ni and Cr have almost the same atomic size; therefore, the effect of the mechanical component is not apparent in Ni/Cr GB. Although the mechanical component is slightly bigger than the chemical one for H segregation in sites S2 and S5 in Table 2, the chemical component plays a dominant role for H in sites S1, S3, S4, and S6 of Ni/Cr GB and results in the overall suppression effect of Cr, which can be inferred from the results in Table 1. As a result, the effects of Cr and Mo on H segregation are mainly attributed to the chemical component.

Since GB serves as a rapid channel for H atoms to diffuse, the effects of alloy compositions on H migration along and across GB were investigated further, and the calculated diffusion barriers for H along and across pure, Ni/Cr, and Ni/Mo GBs are illustrated in Fig. 5 and 6, respectively. Our calculated diffusion barrier of H in pure Ni GB is in reasonable agreement with the results in Ref. [44].

As stated above, there are only three stable sites (i.e., S1, S2, and S5) in one cavity of the GB plane in Ni/Cr and Ni/Mo GBs, and the S2 and S5 sites are equivalent. Therefore, in one cavity surrounded by the 1a, 1b, and 1c atoms illustrated in Fig. 1(b), the diffusion barriers for S1 to S2 and S2 to S1 were calculated and are illustrated in Fig. 5. It is apparent that there are only negligible changes in these diffusion barriers in pure, Ni/Cr and Ni/Mo GBs, and the diffusion barriers are so low that H atoms can move readily within one cavity even in Ni/Cr and Ni/Mo GBs. Although the isosurfaces of optimal charge density are shrunk in Ni/Cr and Ni/Mo GBs in Fig. 4(b) and (c), S1, S2, and S5 are still on these isosurfaces, and the pathways for S1 to S2 and S2 to S1 are still included in these isosurfaces. Thus, the diffusion barriers change slightly in pure, Ni/Cr, and Ni/Mo GBs.

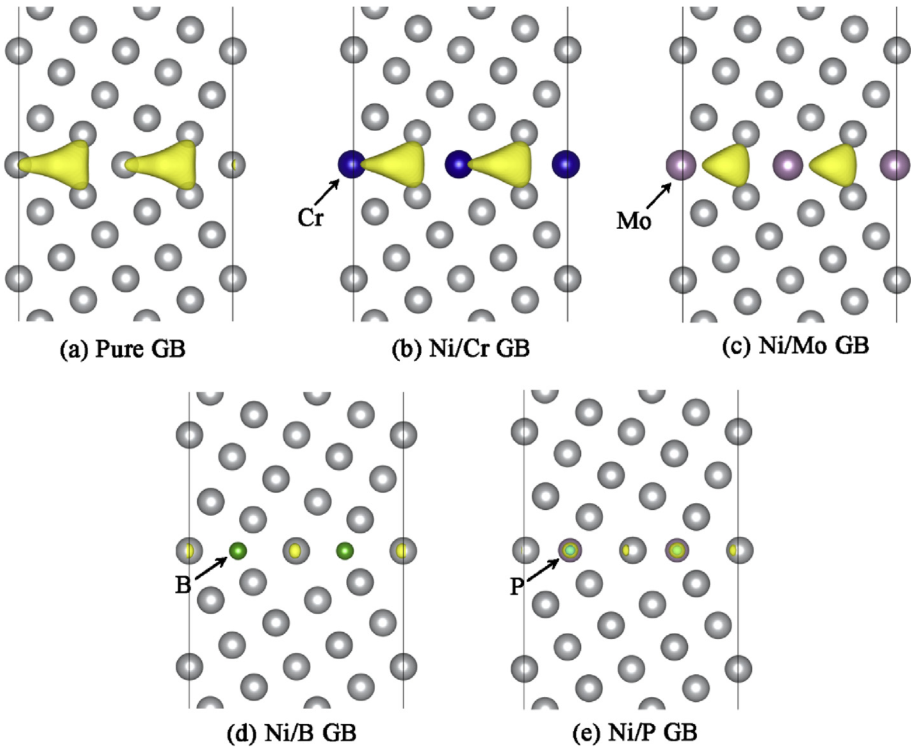

(a) Pure GB (b) Ni/Cr GB (c) Ni/Mo GB

(d) Ni/B GB (e) Ni/P GB

Fig. 4 – The calculated isosurfaces of optimal charge densities for H in (a) pure GB, (b) Ni/Cr GB, and (c) Ni/Mo GB. The calculated results for (d) Ni/B and (e) Ni/P GBs are illustrated for convenience. The isosurface of optimal charge density is 0.021 electrons/Bohr^3 (i.e., 0.14 electrons/Å^3) [44] and is yellow in colour. (For interpretation of the references to color in this figure legend, the reader is referred to the Web version of this article.)

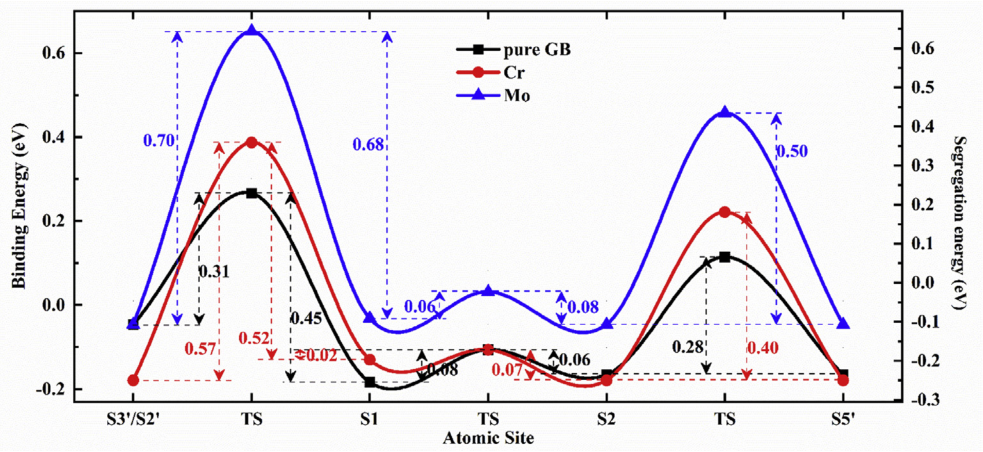

Fig. 5 – **Calculated diffusion barriers for H migration along Ni Σ5 GB, along with the binding energies and the corresponding segregation energies for H (see Fig. 1(a) and (b) to find the atomic positions).**

H migrations from one cavity to an adjacent cavity were also calculated, as illustrated in Fig. 5. For the case of pure GB, the calculated migration paths are S3′ to S1, S1 to S3′, S2 to S5′, and S5′ to S2. Since S3′ is not stable in Ni/Cr and Ni/Mo GBs, the calculated migration paths are S2′ to S1, S1 to S2′, S2 to S5′, and S5′ to S2, as illustrated in Fig. 5. Different from the negligible effects of Cr and Mo on H diffusions within one cavity, Mo and Cr effectively increase the H diffusion barriers between two neighboring cavities, and the effect of Mo is most evident. For example, the H diffusion barriers for S2 to S5’ are 0.28, 0.40, and 0.50 eV in pure, Ni/Cr, and Ni/Mo GBs, respectively. During these processes, H atoms have to diffuse across the iso-surfaces of optimal charge density, resulting in the much higher diffusion barrier. Since H diffusion barriers between adjacent cavities are much larger than those within one cavity as displayed in Fig. 5, the former barriers should be thought of as the determining barriers for H diffusion along the GB plane. As a result, Mo and Cr act as an obstacle for H diffusion along the GB plane.

Furthermore, H diffusions across Ni GB were investigated and the corresponding diffusion barriers are illustrated in Fig. 6. The H migration path is S6 to S6’. In Ni/Cr and Ni/Mo GBs, only sites S1, S2, and S5 sites are stable. Thus, H atoms can jump through these sites during the migration path, and the diffusion barriers of both paths were calculated. As displayed in Fig. 6, these two pathways are more complex, and the upper limits of the energy barriers in one pathway are the determining barriers for H diffusion across the GBs.

For the case of pure GB, when H diffuses from S6′ to S6, it has to overcome the uppermost energy barrier of 0.25 eV through the S1 site and 0.14 eV through the S2 and S5 sites. Thus, the pathway through S1 is preferential with the low energy barrier of 0.14 eV. In Ni/Cr and Ni/Mo GBs, the uppermost energy barriers through S1 decrease to 0.12 and 0.11 eV, respectively, and the uppermost energy barriers through S2/S5 become 0.13 and 0.10 eV, respectively. Thus, the preferred H pathways in Ni/Cr and Ni/Mo GBs are S6’→S1→S6 with a barrier of 0.117 eV and S6’→S2/S5→S6 with 0.10 eV, respectively. As a result, Cr and Mo somewhat reduce the H energy barriers across GBs, compared with the pure GB. Nevertheless, Cr and Mo decrease the H segregation energies in the positive direction in the GB region as discussed earlier and presented in Table 1 and Fig. 6. Thus, Cr and Mo can

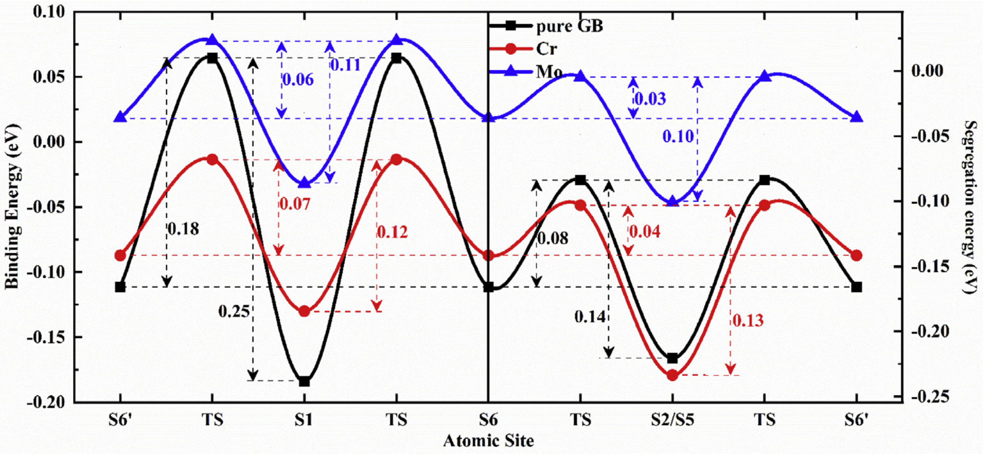

Fig. 6 – **Calculated diffusion barriers for H migration across Ni Σ5 GB along with the binding energies and the corresponding segregation energies for H (see Fig. 1(a) and (b) to find the atomic positions).**

Table 3 – The calculated binding energies and segregation energies (in eV) of H atoms at the O_{GB}/O_{GB}' site of the pure, Ni/Cr, and Ni/Mo CTBs. The segregation energies are in parentheses. The calculated results for Ni/B and Ni/P CTBs are also presented in Table 3 for convenience (See Fig. 1(c) to find the position of O_{GB} and O_{GB}').

	Pure CTB	Ni/Cr CTB	Ni/Mo CTB	Ni/B CTB	Ni/P CTB
O_{GB}/ O_{GB}'	0.06 (−0.01)	0.12 (0.05)	0.38 (0.31)	0.85 (0.79)	1.06 (1.00)

suppress H segregation in the GB region, which can offset the reduced H diffusion barriers.

H at the Ni/B and Ni/P GBs

In the Ni/B and Ni/P GBs, B and P atoms have the strong tendency to accumulate into the GB plane and occupy the GB0 site, with the segregation energy −2.03 and −1.35 eV, respectively, as demonstrated in Fig. 2. By contrast, as presented in Table 1, H segregation energies in pure GB are only −0.24 −0.22 −0.10, and −0.17 eV in sites S1, S2/S5, S3/S4, and S6, respectively, which is much lower than those of B and P. As a result, B and P segregate into the GB region more preferentially than H does.

In Fig. 1(a) and (b), the GB0 site is in the middle of the triangle formed by 1a, 1b, and 1c atoms. Our calculated results indicated that this cavity is too small to accumulate one B (or P) and one H atoms in the meantime. When B or P atoms occupy GB0 sites, it will be unfavorable for H atoms to occupy sites S1, S2/S5, or S3/S4 energetically. Furthermore, when B or P atoms occupy the sites in the GB plane, S6 and S6' become unstable sites for H atoms, and H atoms diffuse away from the GB plane. As illustrated in Fig. 4(d) and (e), in the Ni/B and Ni/P GBs, the calculated isosurfaces of optimal charge densities for H almost disappear because of the existence of B and P segregation, which is different from the cases of pure, Ni/Cr, and Ni/Mo GBs. As a result, the B and P atoms in the GB region can repel H atoms and hinder H segregation into GB more effectively, which may be a possible method of reducing the susceptibility of Ni alloys to HE.

H trapping and diffusion in Ni CTBs with alloy compositions

H at the Ni/Cr and Ni/Mo CTBs

The binding energies of H atom at the O_{GB}/O_{GB}' site of the pure, Ni/Cr and Ni/Mo CTBs were calculated and listed in Table 3.

Table 4 – The calculated total effects of Cr and Mo on H binding energies and segregation energies (in eV) in the O_{GB}/O_{GB}' site of Ni/Cr and Ni/Mo CTBs and the corresponding chemical and mechanical components. The calculated results for Ni/B and Ni/P CTBs are also presented.

	Chemical	Mechanical	Total
At Ni/Cr CTB	−0.10	0.16	0.06
At Ni/Mo CTB	0.83	−0.51	0.32
At Ni/B CTB	0.42	0.37	0.79
At Ni/P CTB	1.48	−0.48	1.00

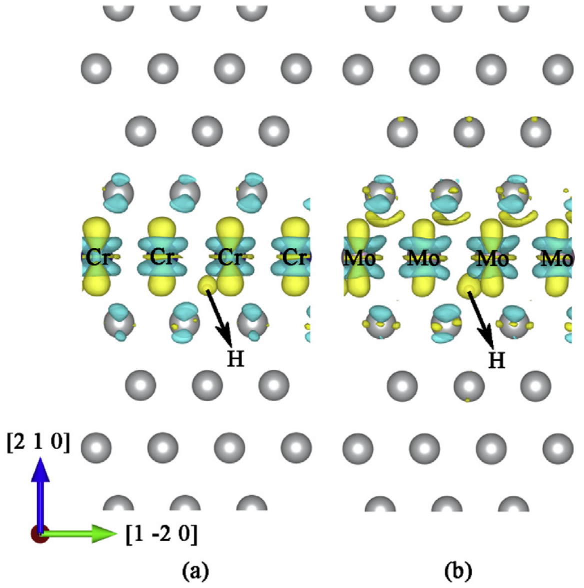

Fig. 7 – The calculated charge density differences in Ni/Cr and Ni/Mo CTBs with one H atom in the OGB site, according to Eq. (5). With the values of 0.006 and −0.006 electrons/ $Bohr^3$, the yellow and blue isosurfaces represent gain and loss of electrons, respectively. The gray balls denote Ni atoms. (For interpretation of the references to color in this figure legend, the reader is referred to the Web version of this article.)

There are no atomic sites in the CTB plane for H atoms to occupy, and the O_{GB} and O_{GB}' sites are the nearest sites to the GB plane. As shown in Table 3, the calculated segregation energy of

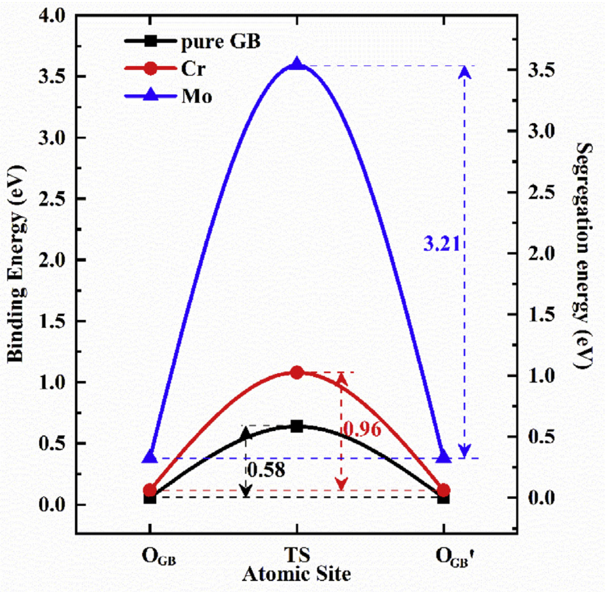

Fig. 8 – Calculated diffusion barriers for H migration from the O_{GB} site to the O_{GB}' site across pure Ni, Ni/Cr, and Nr/Mo CTBs, along with the binding energies and the corresponding segregation energies for H (see Fig. 1(c) to find the positions of O_{GB} and O_{GB}'). 'TS' denotes transition state.

H at the O_{GB}/O_{GB}' site of pure CTB is −0.01 eV, meaning that the H segregation and trapping in pure CTB is negligible. Additionally, the H binding energies are all positive and in the order pure CTB < Ni/Cr < Ni/Mo; thus, Mo in CTB mostly repels H, which is in accordance with that in the case of GB.

As displayed in Table 4, Cr and Mo increase the H binding energies and segregation energies by 0.06 and 0.32 eV in Ni/Cr and Ni/Mo GBs, respectively, compared with in pure Ni GB. The effect of Cr is negligible, whereas that of Mo is more obvious. The mechanical component of Mo is negative with the value of −0.51 eV and promotes H segregation, which is directly associated with the volume expansion induced by the large atomic size of Mo. Nevertheless, the chemical component plays a dominant role with the value of 0.83 eV, which is in good agreement with the role of Mo in the GB case as stated above.

While the isosurface of optimal charge density in GB can induce H accumulation on the internal surface as stated above, there are no cavities that can provide these isosurfaces in CTB; this is confirmed by the calculated charge densities of the pure, Ni/Cr, Ni/Mo, Ni/B, and Ni/P CTBs. As a result, there are no apparent tendencies for H atoms to segregate into the CTB plane, which agrees with the results in Table 3. Since the isosurface of optimal charge density cannot be used to study the differences in the chemical components of Cr and Mo in Table 4, the charge density differences were calculated and are illustrated in Fig. 7. The charge density differences, ρ, were calculated as follows:

$$\rho = [\rho(AlloyedCTB) - \rho(pureCTB)] - [\rho(Alloy) - \rho(Ni)], \quad (5)$$

where $\rho(pureCTB)$ is the charge density of pure Ni CTB with the H atom in the O_{GB} site. Since the atomic positions of Ni/Cr and Ni/Mo CTBs are close to those of pure CTB, $\rho(AlloyedCTB)$ denotes the charge density of pure Ni CTB with the H atom in the O_{GB} site in which Ni atoms in CTB1 sites are replaced by Cr or Mo atoms. $\rho(Alloy)$ indicates the charge density of the Cr or Mo monolayer in CTB1 sites, and $\rho(Ni)$ is that of the Ni monolayer in CTB1 sites.

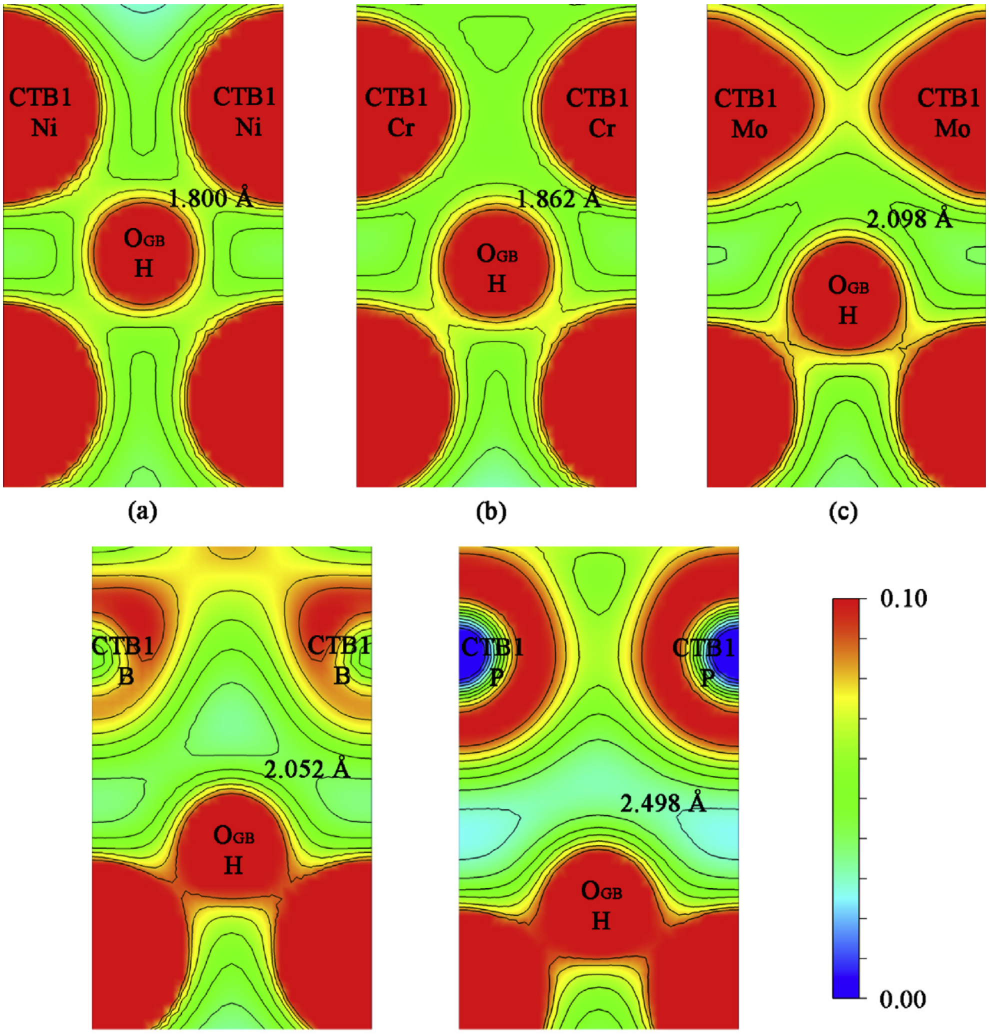

Fig. 9 – The calculated valence charge density distributions (electrons/Bohr^3) for (a) pure GB, (b) Ni/Cr GB, (c) Ni/Mo GB, (d) Ni/B GB and (e) Ni/P GB with an H atom in the O_{GB} site. The H atom in the O_{GB} site and the Ni atoms in the CTB1 sites (or the corresponding substitute elements) are in this plane of charge density. The calculated distances between H in the O_{GB} site and the atom in the CTB1 site (i.e., Ni, Cr, Mo, B, or P) are also displayed.

As shown in Fig. 7, Cr and Mo segregations in the CTB planes induce the charge accumulation around H atoms and that H atoms gain more electrons from Cr and Mo than Ni in the CTB plane. Particularly, more electrons can be found around the H atom in Ni/Mo CTB, meaning that the chemical effect of Mo is more obvious than that of Cr. More obvious charge accumulation in Ni/Mo CTB makes H segregation more difficult; this can be used to interpret the chemical component of Mo in Table 4, because H atoms tend to stay in a position with low electron density and the charge density of optimal isosurface for H is very low.

After Cr and Mo occupy the CTB1 sites, the H binding energies in O_{GB} and O_{GB}' sites are largely increased as listed in Table 3. Furthermore, the diffusion barriers for H migration across pure Ni, Ni/Cr, and Nr/Mo CTBs were calculated and illustrated in Fig. 8, with the values of 0.58, 0.96, and 3.21 eV, respectively. Thus, it is easiest for H to diffuse across pure Ni CTB and most difficult to diffuse across Ni/Mo CTB, and the large diffusion barrier (3.21 eV) makes it impossible for H to diffuse across Ni/Mo CTB, so Mo atoms act as an obstacle for H diffusion.

H at the Ni/B and Ni/P CTBs

Table 3 presents the calculated H binding energies at the O_{GB}/O_{GB}' site of the Ni/B and Ni/P CTBs. Compared with the cases of pure, Ni/Cr, and Ni/Mo CTBs, the H binding energies increase further into 0.85 and 1.06 eV in Ni/B and Ni/P CTBs, respectively, indicating that B and P repel H more obviously than Cr and Mo. It can be seen in Table 4 that the chemical components of B and P play a dominant role with the values of 0.42 and 1.48 eV, respectively. To shed light on the chemical components of the effects of B and P on H behaviors, the calculated charge densities in Ni/B and Ni/P CTBs are displayed in Fig. 9 in comparison with those in pure Ni, Ni/Cr and Ni/Mo CTBs.

Although the calculated distances between H in the O_{GB} site and the metal atoms in the CTB1 site increase gradually with the increase of atomic sizes of Ni, Cr, and Mo from Fig. 9(a)–(c), the Ni–H, Cr–H and Mo–H bonds have no qualitative changes as judged by the charge density distributions between them. However, in Fig. 9(d) and (e), the charge densities between B (or P) and H become much more diluted than the corresponding ones in Fig. 9(a)–(c). In the meantime, the B–H and P–H distances are lengthened more remarkably in Fig. 9(d) and (e) as compared with the corresponding distances in Fig. 9(a), (b), and (c). Thus, it can be concluded that the B–H and P–H bonds are very weak and almost negligible.

Because of their large electronegativity, B, P, and H can obtain electrons from the adjacent Ni atoms by binding with them and forming a relatively stable electronic configuration. As a result, the neighboring B, P, and H do not tend to bind with each other as judged by the dilute charge density

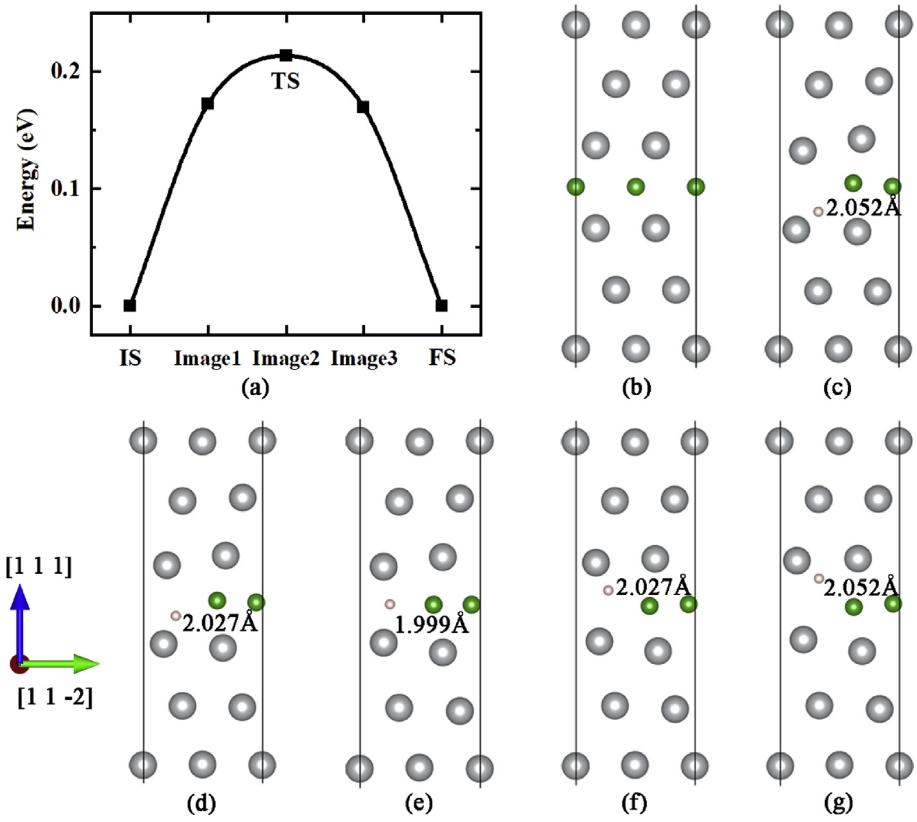

Fig. 10 – (a) Calculated diffusion barriers for H migration from O_{GB} to O_{GB}' across the plane of Ni/B CTB, along with the corresponding atomic configurations (c) Initial state (IS), (d) Image1, (e) Image2, (f) Image3 and (g) Final state (FS) in the process of H migration. (b) Is the calculated atomic configuration of Ni/B CTB without H atoms. The distances between H and the nearest B are also presented. The gray, green and pink balls denote Ni, B and H atoms, respectively. (For interpretation of the references to color in this figure legend, the reader is referred to the Web version of this article.)

between them in Fig. 9(d) and (e). Actually, the B–H and P–H interactions can be interpreted a repulsive force that is illustrated by the interactions between the two neighboring S atoms [30] and P atoms [52]; this force is also applicable to the B–H interaction illustrated in Fig. 9(d). The charge density between B in the CTB1 site and H in O_{GB} in Fig. 9(d) is denser than that between P in the CTB1 site and H in O_{GB} in Fig. 9(e); thus, the repulsive force between P and H atoms is stronger than that between B and H atoms, which is accordance with the calculated results that the P–H distance in Fig. 9(e) is longer than the B–H distance in Fig. 9(d).

The diffusion barriers for H migration from O_{GB} to O_{GB}' across the CTB planes in Ni/B and Ni/P CTBs were calculated. The calculated H diffusion barrier in Ni/B CTB is 1.06 eV and displayed in Fig. 10, along with the corresponding atomic configurations in the diffusion process. In the diffusion process from Fig. 10(c)–(g), the B–H balance distance remains almost the same (approximately 2 Å) as in Fig. 9(d). The atomic size of B is much smaller than those of Ni, Cr, and Mo, and the region near the CTB plane is large enough to accommodate the B–H balance distance, which can relieve the repulsive interaction between B and H. As a consequence, the H diffusion barrier in Ni/B CTB is lower than that in Ni/Mo CTB because of the much smaller atomic size of B than that of Mo and is higher than in pure and Ni/Cr CTBs because of the B–H repulsive interaction.

The H diffusion barrier in Ni/P CTB was calculated to be more than 10 eV, indicating that P acts as a strong obstacle to H diffusion in Ni/P CTB. Since the atomic size of P is larger than that of B, the region near the CTB plane cannot accommodate the balance distance between P and H with the value of 2.498 Å illustrated in Fig. 9(e). Consequently, the P–H repulsive interaction cannot be relieved and play a dominant role in the H diffusion process.

Conclusions

First-principles calculations have been carried out to study the effects of common metallic and nonmetal alloy compositions (i.e., Cr, Mo, B, and P) on hydrogen behaviors at the nickel grain boundary (GB) and the coherent twin boundary (CTB). H segregation and diffusion in GB and CTB were investigated to explore the physical mechanism of the effects of alloy compositions. The key findings are listed as follows:

1. H, Cr, Mo, B, and P have a stronger segregation into Ni GB than Ni CTB because of the presence of the cavity in GB.
2. Cr and Mo suppress H segregation and diffusion in Ni GB. Particularly, the shrinkage of isosurfaces of optimal charge densities for H plays a dominant role in the effect of Mo.
3. B and P have a much stronger tendency to accumulate into the GB plane than that of H; this is a strong competitive effect to H segregation and diffusion.
4. Charge accumulations induced by Cr and Mo in Ni CTB make these atoms act as an obstacle for H segregation and diffusion.
5. The B–H and, especially, P–H repulsive interactions inhibit H segregation and diffusion in Ni CTB.

The present study provides the microscopic images of H segregation and diffusion in Ni GB and CTB under the influence of several common and typical alloy compositions, which is essential for understanding the mechanism of hydrogen embrittlement (HE) and improving the ability of alloys against HE and can serve as a necessary complement to the experimental work.

Acknowledgments

This work is supported by National Natural Science Foundation of China (Grant No. 51601212, 11832019, 11472313 and 11572355).

REFERENCES

[1] Louthan MR, Rawl DE, Caskey GR, Donovan JA. Hydrogen embrittlement of metals. Mater Sci Eng 1972;10:357–68.
[2] Barnoush A, Vehoff H. Recent developments in the study of hydrogen embrittlement: hydrogen effect on dislocation nucleation. Acta Mater 2010;58(16):5274–85.
[3] Zhou X, Mousseau N, Song J. Is hydrogen diffusion along grain boundaries fast or slow? Atomistic origin and mechanistic modeling. Phys Rev Lett 2019;122:21.
[4] Dwivedi SK, Vishwakarma M. Hydrogen embrittlement in different materials: a review. Int J Hydrogen Energy 2018;43(46):21603–16.
[5] Koyama M, Akiyama E, Lee Y-K, Raabe D, Tsuzaki K. Overview of hydrogen embrittlement in high-Mn steels. Int J Hydrogen Energy 2017;42(17):12706–23.
[6] Ohaeri E, Eduok U, Szpunar J. Hydrogen related degradation in pipeline steel: a review. Int J Hydrogen Energy 2018;43(31):14584–617.
[7] Dwivedi SK, Vishwakarma M. Effect of hydrogen in advanced high strength steel materials. Int J Hydrogen Energy 2019;44(51):28007–30.
[8] Chen Y-S, Lu H, Liang J, Rosenthal A, Liu H, Sneddon G, McCarroll I, Zhao Z, Li W, Guo A, Cairney JM. Observation of hydrogen trapping at dislocations, grain boundaries, and precipitates. Science 2020;367(6474):171–5.
[9] Barrera O, Bombac D, Chen Y, Daff TD, Galindo-Nava E, Gong P, Haley D, Horton R, Katzarov I, Kermode JR, Liverani C, Stopher M, Sweeney F. Understanding and mitigating hydrogen embrittlement of steels: a review of experimental, modelling and design progress from atomistic to continuum. J Mater Sci 2018;53(9):6251–90.
[10] Li X, Gao M, Li H, Xing W, Zhang L, Shu L, Zhao X, Ma Y, Liu K. Effect of residual hydrogen content on the tensile properties and crack propagation behavior of a type 316 stainless steel. Int J Hydrogen Energy 2019;44(45):25054–63.
[11] Noh H-S, Kang J-H, Kim S-J. Effect of grain size on hydrogen embrittlement in stable austenitic high-Mn TWIP and high-N stainless steels. Int J Hydrogen Energy 2019;44(45):25076–90.
[12] Chen Y-S, Bagot PAJ, Moody MP, Haley D. Observing hydrogen in steel using cryogenic atom probe tomography: a simplified approach. Int J Hydrogen Energy 2019;44(60):32280–91.
[13] Zhu L, Zhou J, Yang H, Sun Z. Energetics and kinetics of hydrogen at the grain boundary of the Ni alloys: a first-principles study. J Alloys Compd 2019;795:343–50.

[14] Zhou X, Marchand D, McDowell DL, Zhu T, Song J. Chemomechanical origin of hydrogen trapping at grain boundaries in fcc metals. Phys Rev Lett 2016;116:075502.

[15] Alvaro A, Jensen IT, Kheradmand N, Lovvik OM, Olden V. Hydrogen embrittlement in nickel, visited by first principles modeling, cohesive zone simulation and nanomechanical testing. Int J Hydrogen Energy 2015;40(47):16892–900.

[16] Mattsson TR, Wahnstrom G, Bengtsson L, Hammer B. Quantum-mechanical calculation of H on Ni(001) using a model potential based on first-principles calculations. Phys Rev B 1997:2258–66.

[17] Greeley J, Mavrikakis M. A first-principles study of surface and subsurface H on and in Ni(111): diffusional properties and coverage-dependent behavior. Surf Sci 2003;540(2–3):215–29.

[18] Wimmer E, Wolf W, Sticht J, Saxe P, Geller CB, Najafabadi R, Young GA. Temperature-dependent diffusion coefficients from ab initio computations: hydrogen, deuterium, and tritium in nickel. Phys Rev B 2008;77:13.

[19] Torres E, Pencer J, Radford DD. Atomistic simulation study of the hydrogen diffusion in nickel. Comput Mater Sci 2018;152:374–80.

[20] Di Stefano D, Mrovec M, Elsaesser C. First-principles investigation of quantum mechanical effects on the diffusion of hydrogen in iron and nickel. Phys Rev B 2015;92:22.

[21] Fullarton ML, Voskoboinikov RE, Middleburgh SC. Hydrogen accommodation in alpha-iron and nickel. J Alloys Compd 2014;587:794–9.

[22] Tanguy D, Wang Y, Connetable D. Stability of vacancy-hydrogen clusters in nickel from first-principles calculations. Acta Mater 2014;78:135–43.

[23] Connetable D, Wang Y, Tanguy D. Segregation of hydrogen to defects in nickel using first-principles calculations: the case of self-interstitials and cavities. J Alloys Compd 2014;614:211–20.

[24] Metsue A, Oudriss A, Feaugas X. Trapping/detrapping kinetic rates of hydrogen around a vacancy in nickel and some consequences on the hydrogen-vacancy clusters thermodynamic equilibrium. Comput Mater Sci 2018;151:144–52.

[25] Wang Y, Connetable D, Tanguy D. Influence of trap connectivity on H diffusion: vacancy trapping. Acta Mater 2016;103:334–40.

[26] Geng WT, Freeman AJ, Olson GB, Tateyama Y, Ohno T. Hydrogen-promoted grain boundary embrittlement and vacancy activity in metals: insights from ab initio total energy calculations. Mater Trans 2005;46(4):756–60.

[27] Geng WT, Freeman AJ, Wu R, Geller CB, Raynolds JE. Embrittling and strengthening effects of hydrogen, boron, and phosphorus on a Sigma 5 nickel grain boundary. Phys Rev B 1999;60(10):7149–55.

[28] He S, Ecker W, Pippan R, Razumovskiy VI. Hydrogen-enhanced decohesion mechanism of the special Sigma 5(012) 100 grain boundary in Ni with Mo and C solutes. Comput Mater Sci 2019;167:100–10.

[29] Huang S, Chen D, Song J, McDowell DL, Zhu T. Hydrogen embrittlement of grain boundaries in nickel: an atomistic study. npj Comput Mater 2017;2:1–7.

[30] Yamaguchi M, Shiga M, Kaburaki H. Grain boundary decohesion by impurity segregation in a nickel-sulfur system. Science 2005;307(5708):393–7.

[31] Lu L, Chen X, Huang X, Lu K. Revealing the maximum strength in nanotwinned copper. Science 2009;323(5914):607–10.

[32] Lu K. The future of metals. Science 2010;328(5976):319–20.

[33] Fan TW, Wang ZP, Lin JJ, Chen DC, Fang QH, Hu T, Nie BH, Wang K, Hu HW, Sun HB, He HY, Ma L, Tang PY. First-principles predictions for stabilizations of multilayer nanotwins in Al alloys at finite temperatures. J Alloys Compd 2019;783:765–71.

[34] Zhang Z, Sheng H, Wang Z, Gludovatz B, Zhang Z, George EP, Yu Q, Mao SX, Ritchie RO. Dislocation mechanisms and 3D twin architectures generate exceptional strength-ductility-toughness combination in CrCoNi medium-entropy alloy. Nat Commun 2017;8:14390.

[35] Zhou X, Song J. Effects of alloying elements on vacancies and vacancy-hydrogen clusters at coherent twin boundaries in nickel alloys. Acta Mater 2018;148:9–17.

[36] Liu W, Qian Y, Zhang D, Zeng Y, Han X, Chu X, Yin H, Yang G, Wang G, Wu S, Liu W. A theoretical study of the effects of sp-elements on hydrogen in nickel-based alloys. Comput Mater Sci 2017;128:37–41.

[37] Liu W, Qian Y, Zhang D, Liu W, Han H. First-principles calculations of the interaction between hydrogen and 3d alloying atom in nickel. J Nucl Mater 2015;465:254–9.

[38] Liu WG, Qian Y, Zhang DX, Han X-B, Chu X-X, Zeng Y-S, Bao G-L, Wang G-H, Wu SW, Liu W. Theoretical study of the interaction between hydrogen and 4d alloying atom in nickel. Nucl Sci Tech 2017;28(6):119–22.

[39] Kresse G, Furthmuller J. Efficient iterative schemes for ab initio total-energy calculations using a plane-wave basis set. Phys Rev B 1996;54(16):11169–86.

[40] Hohenberg P, Kohn W. Inhomogeneous electron gas. Phys Rev B 1973;7(5):1912–9.

[41] Kohn W, Sham LJ. Self-consistent equations including exchange and correlation effects. Phys Rev 1965;140(4A):1133.

[42] Blochl PE. Projector augmented-wave method. Phys Rev B 1994;50(24):17953–79.

[43] Perdew JP, Chevary JA, Vosko SH, Jackson KA, Pederson MR, Singh DJ, Fiolhais C. Atoms, molecules, solids, and surfaces: applications of the generalized gradient approximation for exchange and correlation. Phys Rev B 1992;46(11):6671–87.

[44] Di Stefano D, Mrovec M, Elsaesser C. First-principles investigation of hydrogen trapping and diffusion at grain boundaries in nickel. Acta Mater 2015;98:306–12.

[45] Henkelman G, Uberuaga BP, Jonsson H. A climbing image nudged elastic band method for finding saddle points and minimum energy paths. J Chem Phys 2000;113(22):9901–4.

[46] Henkelman G, Jonsson H. Improved tangent estimate in the nudged elastic band method for finding minimum energy paths and saddle points. J Chem Phys 2000;113(22):9978–85.

[47] Liu W, Han H, Ren C, Yin H, Zou Y, Huai P, Xu H. Effects of rare-earth on the cohesion of Ni Sigma 5 (012) grain boundary from first-principles calculations. Comput Mater Sci 2015;96:374–8.

[48] Liu W, Ren C, Han H, Tan J, Zou Y, Zhou X, Huai P, Xu H. First-principles study of the effect of phosphorus on nickel grain boundary. J Appl Phys 2014;115(4):043706.

[49] Vsianska M, Sob M. The effect of segregated sp-impurities on grain-boundary and surface structure, magnetism and embrittlement in nickel. Prog Mater Sci 2011;56(6):817–40.

[50] He B, Xiao W, Hao W, Tian Z. First-principles investigation into the effect of Cr on the segregation of multi-H at the Fe Sigma 3 (111) grain boundary. J Nucl Mater 2013;441(1–3):301–5.

[51] Zhou HB, Liu YL, Jin S, Zhang Y, Luo GN, Lu GH. Investigating behaviours of hydrogen in a tungsten grain boundary by first principles: from dissolution and diffusion to a trapping mechanism. Nucl Fusion 2010;50(2):025016.

[52] Liu WG, Ren CL, Han H, Tan J, Zou Y, Zhou XT, Huai P, Xu HJ. First-principles study of the effect of phosphorus on nickel grain boundary. J Appl Phys 2014;115(4):043706.